Green Chemistry

Accepted Manuscript

Stille couplings in water @RT

ROYAL SOCIETY OF CHEMISTRY

www.rsc.org/greenchem

Green Chemistry

ARTICLE

Biocompatible Reduced Graphene Oxide Sheets with Superior Water Dispersibility Stabilized by Cellulose Nanocrystal and Their Polyethylene Oxide Composites

Yun-Sheng Ye,[*a] Hong-Xia Zeng,[a] Jun Wu,[a] Li-Yun Dong,[b] Jin-Tao Zhu[a], Zhi-Gang Xue,[a] Xing-Ping Zhou,[a] Xiao-Lin Xie[*a] and Yiu-Wing Mai[c]

Organic molecular and polymeric stabilizers are useful for preparing individually dispersed graphene sheets, thus offering new possibilities for the production of nanomaterials. Although exfoliated graphene flakes with good dispersibility can be produced, their use in polymer composites remains limited due to their low stabilty and mechanical strength. In this work, stable high concentration aqueous dispersions (>10 mg mL^{-1}) of reduced graphene oxide (RGO) sheets were prepared by exfoliation/*in-situ* reduction of graphene oxide (GO) in the presence of cellulose nanocrystals (CNC). The sandwich-like structure formed with the hydrophilic outer surface of CNC forms CNC decorated RGO (CNC-RGO) which is easily dispersed in water with a high thermal stability (> 320 °C) comparable to pristine CNC and other common stabilizers. Polyethylene oxide (PEO) based nanocomposites, using fully exfoliated CNC-RGO hybrids, were prepared with a simple procedure. The PEO/CNC-RGO composite films show superior mechanical properties compared to PEO composite films enhanced by other small molecules, polymer dispersants, stabilized RGO or pristine CNC. Not only are the elastic modulus and tensile strength of the composites significantly improved, their thermal stability is also retained. The hydrothermal dehydration of GO to RGO, using biodegradable and renewable materials such as CNC, offers a "*green approach*" to large-scale preparation of highly biocompatible and easily dispersed RGO for a range of applications.

Introduction

Graphene-based materials have received much attention due to their outstanding physical properties.[1] To use such materials in specific end applications, including batteries, sensors, super capacitors and polymer nanocomposites, we must preserve the intrinsic physical properties of graphene, while homogeneously incorporating it into various matrices. For the large scale production of graphene-based materials, a widely adopted strategy is to use chemically exfoliated graphene oxide (GO)[2], prepared by oxidizing graphite with strong oxidants, and then converting it to reduced graphene oxide (RGO).[3, 4] However, the processes used to produce thermally/chemically-converted graphene (TCG/CCG) usually results in its incompatibility with hydrophilic or hydrophobic media, leading to re-stacking or re-aggregation, which affects

adversely its potential for applications in polymer composites.

To address this problem, functionalization of TCG/CCG is widely used to improve its dispersibility and compatibility with different types of liquid/solid media and target matrices, which in general can be grouped into two main categories: those with covalent, and those with non-covalent functionalizations.[1, 5, 6] Both approaches to functionalize RGO sheets provide good dispersions, which are compatible with a target matrix. However, non-covalent functionalization of graphene/RGO that uses intermolecular interactions to bind graphene and the stabilizers has the advantage of avoiding complicated chemical processes. This is recognized as an effective method for modifying graphene/RGO without destroying its conjugated structure. Recently, there have been numerous reports of graphite and RGO decorated with small organic molecules or polymers which have shown that the resulting graphene/RGO can form a stable suspension in organic or aqueous media.[7, 8] For example, some polymer molecules, such as poly(sodium 4-styrenesulfonate) (PSS)[9], sulfonated polyaniline (SPAN)[10], amine terminated polystyrene[11], amphiphilic coil-rod-coil conjugated tri-block copolymer[12], single-stranded DNA[13], polyoxometalates[14], polymeric ionic liquid (PIL)[15, 16] and pyrene-terminated polymer[17-19], have been used as stabilizers to modify graphene/RGO by exploiting their π-stacking or electrostatic interactions. However, most reported approaches are environmentally unsustainable. Hence, in response, many attempts have been made to develop environmentally friendly

[a.] *Key Laboratory for Large-Format Battery Materials and System, Ministry of Education, School of Chemistry and Chemical Engineering, Huazhong University of Science and Technology, Wuhan 430074, China*
[b.] *Department of Dermatology, Affiliated Union Hospital, Tongji Medical College, Huazhong University of Science and Technology (HUST), Wuhan 430022, China*
[c.] *Centre for Advanced Materials Technology (CAMT), School of Aerospace, Mechanical and Mechatronic Engineering J07, The University of Sydney, Sydney, NSW 2006, Australia*
† Footnotes relating to the title and/or authors should appear here.
Electronic Supplementary Information (ESI) available: [details of any supplementary information available should be included here]. See DOI: 10.1039/x0xx00000x

approaches for the fabrication of water/organic-dispersible RGO sheets. Biomolecules such as dextran[20], dopamine[21, 22], ascorbic acid[23], vitamin C[24], tannin[25], gallic acid[26], heparin[27] and glucose[28] have been used as reducing agents or stabilizers. However, the dispersibility of the corresponding RGO has rarely been investigated. The dispersible concentration of RGO in the resulting dispersions is usually less than 1.0 mg mL^{-1}, which is somewhat low for practical applications.[6, 7, 9, 29, 30]

Recently, cellulose and its nanocrystalline form, *i.e.*, cellulose nanocrystal (CNC), has attracted much attention due to its unique structure and properties, including its low cost, low density, relatively high thermal stabilization, high sorption capacity, high aspect ratio, large surface area and excellent bio-compatibility, all of which are of utmost importance in fabricating biodegradable advanced materials.[31-33] CNC possesses rigid needle-like crystalline structures which have surface hydroxyl groups[34] making it hydrophilic and thus able to be dispersed in water as stable suspensions of individual fibers, whose basic structure has the advantage that it can form many strong interactions with fillers. It is for this reason that various nanomaterials are based on it.[35-38] In addition, the abundance of reactive hydroxyl groups on CNC surface means it can be modified with various chemical groups, *e.g.,* by esterification, oxidation or polymer grafting; these reactive surface groups also facilitate the incorporation and dispersion of CNC into target polymer matrices.[39-41]

We prepared highly water-dispersible electrically conducting RGO sheets by using CNC as a stabilizer. For comparison, small molecular or polymeric stabilizers were also used to stabilize aqueous RGO during the reduction process to show the advantages of CNC on the resulting physical properties of RGO and their hybrids. The use of CNC as a stabilizer has considerable advantages compared to other stabilizers employed in previous reports. Firstly, CNC can be produced by the acid hydrolysis of cellulose, which is the most abundant biomass material in nature. Secondly, synthesized CNC-RGO hybrids can be re-dispersed in water and organic solvents with high dispersibility (up to ~10 mg mL^{-1} in water), which is the best aqueous dispersibility ever reported for RGO. Thirdly, unlike small molecular surfactants or polymeric dispersants, theoretical and experimental results show that CNC is mechanically stiff with an elastic modulus ~145 GPa in the axial direction.[31] When CNC-RGO hybrids are incorporated into a polyethylene oxide (PEO) matrix, the resulting PEO/CNC-RGO composite films show significant improvements in their mechanical properties. Fourthly, we observed that homogeneous colloidal suspensions of electrical conductive RGO could be produced by hydrothermal dehydration in the presence of CNCs. The relative toxicity of the resulting CNC-RGO hybrid is significantly lower than those reported by using conventionally prepared water dispersible RGO. Hence, we believe that the use of CNC as a stabilizer and the hydrothermal conversion method to produce RGO allows the fabrication of biocompatible RGO and RGO-based nano-composites for a wide range of potential applications.

Results and discussion

To maximize the dispersibility of RGO, the use of different CNC/GO weight ratios in the reduction process was studied. Thus, in a typical procedure, CNC/GO suspensions with various weight ratios, *i.e.,* 1, 3, 6, 10 and 15, were ultra-sonicated and reduced by hydrazine (Table 1). It is well-known that small molecular or polymeric stabilizers that assist RGO are particularly useful for preparing RGO suspensions in water or organic solvents.[16, 19] To show the advantages of CNC as a stabilizer against the reported results for other stabilizers, we undertook control experiments under the same conditions with those widely used for small molecular and polymeric stabilizers, *i.e.,* SDS and PIL (denoted as SDS-RGO and PIL-RGO, respectively) [**Fig. S1 (d)** and **(c)**].[16] After reduction, the excess stabilizer was removed by centrifugation at 13,000 rpm for 0.5 h 3~5 times until no more CNC was detected; this allowed RGO decorated with CNC to be quantified by TGA. In addition, we also examined the ability to exfoliate RGO by direct blending with CNC (CNC/RGO suspension weight ratio 10:1) using the above processes for preparation and purification [Fig S1 (b)].
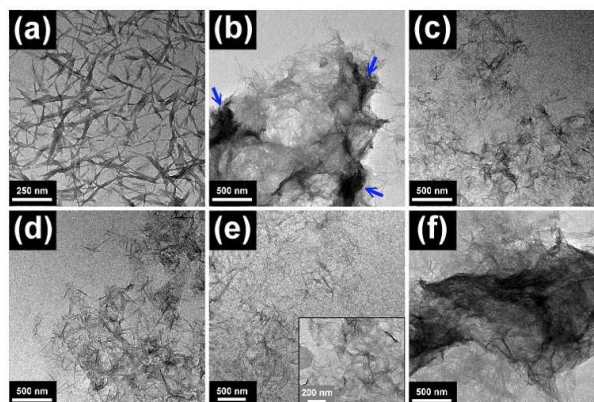

Figure 1. TEM images of (a) pristine CNC, (b) CNC-RGO 1, (c) CNC-RGO 3, (d) CNC-RGO 6, (e) CNC-RGO 10, and (f) CNC/RGO 10 mixture.
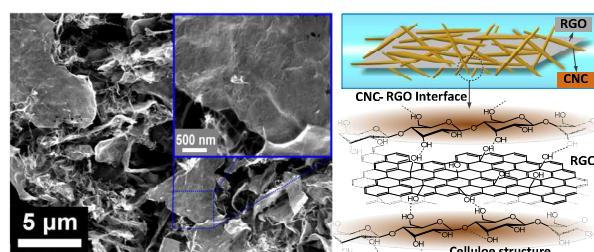
Figure 2. SEM image of CNC-RGO 10 hybrid (left); schematic illustrations of CNC-RGO hybrid (right).

Fig. 1 (a)-(f) shows transmission electron microscopy (TEM) images of very dilute suspensions of pristine CNC, CNC/RGO blend and CNC-RGO hybrids with different starting CNC/RGO ratios deposited on carbon-coated grids. As shown in **Fig. 1(a)**, the pristine CNC was a needle-like crystalline structure 5-15 nm in width and 50-250 nm in length, which is similar to the reported size of CNC formed by sulfuric acid hydrolysis.[42] It is

ARTICLE

well-known that RGO is prone to aggregation after reduction caused by the removal of oxygenated functionalized groups.[4] For the low starting CNC/RGO ratio (CNC-RGO 1), some of the sheets were agglomerated resulting in a folded morphology (marked by the blue arrows in **Fig. 1(b)**) due to insufficient CNC decoration on the RGO surface. As the starting CNC/RGO ratio increases, **Fig. 1(c)-(e)** shows that the RGO sheets are evenly decorated by compact CNC networks, most of them spread on the carbon-coated grids. Scanning electron microscopy (SEM) images of CNC-RGO 10 (**Fig. 2**) display an isotropic structure and very loosely stacked structures with CNC present on the sample surface. The observed morphology shows uniform coverage by a CNC network on the surfaces of the exfoliated RGO sheets in the CNC-RGO hybrid that leads to an integrated network of hybrid material with a sandwich-like structure (**Fig. 2**, right). We speculate that the H-bonding interactions between the GO sheets and CNC induce physical adsorption, and that these interactions are strong enough to overcome the stacking interaction of RGO during reduction.[43] **Fig. 1(f)** shows that a sonicated CNC/RGO mixed sample does not permit RGO exfoliation; the presence of agglomerated RGO sheets hence confirms the importance of *in-situ* CNC/GO reduction.
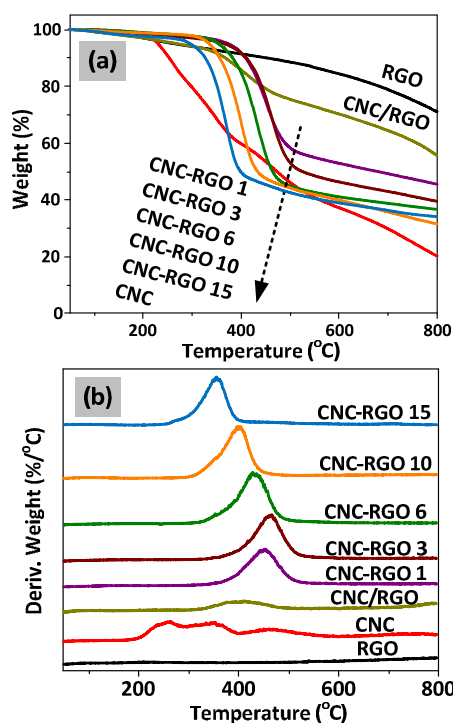

Figure 3. (a) TGA and (b) DTG curves of CNC, CNC/RGO blend and CNC-RGO hybrids.

TGA was used as a complementary technique to reveal the composition and thermal degradation behavior of CNC, CNC/RGO blends and CNC-RGO hybrids (**Fig. 3**). It is observed that CNC is thermally unstable and starts to lose mass upon heating above 200 °C, which is attributed to the remnant sulfate groups on CNCs.[44] By contrast, RGO shows a small mass loss below 200 °C but still displays a mass loss of 10 % at

around 400 °C due to the residual groups on the RGO surface. Its residual weight was about 72%, which is higher than that of pristine CNC (20 %). It should be noted that CNC-RGO hybrids exhibit a higher thermal stability compared to pristine CNC, which is thermally stable until ~320 °C when mass loss starts. This result can be attributed to the compact network structure of CNC, formed on the RGO surface in the CNC-RGO hybrids, which hinders CNC and RGO decomposition. In addition, the TGA curves of CNC-RGO hybrids tend to move towards a low temperature direction with increasing starting CNC/GO ratios. Similarly, the derivative TGA profiles of CNC-RGO hybrids show only one main peak which shifts to lower temperatures from CNC-RGO 1 to CNC-RGO 10 due to the increases in the content of thermally unstable CNC in the CNC-RGO hybrids. For the CNC/RGO blend sample, although the decomposition of CNC is retarded, it is less thermally stable, with a mass loss beginning below 100°C due to the lack of a dense CNC network formed on the RGO surface. We can conclude that the uniform decoration of CNC on the RGO surface benefits nanomaterials suitable for applications demanding high thermal stability.

Table 1. Effect of starting CNC/GO weight ratio on CNC coverage ratio and dispersibility of resulting CNC-RGO hybrids.

Samples	Starting CNC/RGO weight ratio	Coverage ratio (wt%)[a]	Dispersibility (mg mL^{-1})[b]
CNC-RGO 1	1	10.6	0.06
CNC-RGO 3	3	22.2	0.46
CNC-RGO 6	6	28.2	0.70
CNC-RGO 10	10	45.6	2.63
CNC-RGO 15	15	45.2	2.51
CNC-RGO$_{HT}$ 10	10	43.5	2.52

[a] Determined by TGA.
[b] Determined by UV/vis spectroscopy.

Table 1 shows the CNC coverage ratio of CNC-RGO hybrids quantified by TGA and dispersibility of the hybrids obtained for different starting CNC/GO weight ratios. It can be seen that the coverage ratio gradually increases with increasing starting CNC/GO weight ratio from 1 to 10, levelling beyond a weight ratio >10. As described in our previous studies[45, 46], the degree of solubility of carbon-based materials could be estimated by UV/vis spectroscopy. Generally, the absorption properties of graphene-based materials are determined by the absorption at 500 nm in the solution absorption spectra. The CNC-RGO 10 and pristine CNC samples were separately dissolved in water to produce a total of six different samples of varying concentrations; their absorption at 500 nm was plotted against the RGO and CNC concentrations, respectively. The slopes of the "least squares straight lines" provided the specific extinction coefficients for CNC-RGO 10 (0.6558) and pristine CNC (0.0053) which were used to estimate the maximum RGO concentration in the CNC-RGO hybrids. Hence, we found that the specific extinction coefficient of CNC-RGO was much larger than that of CNC; we can, therefore, rule out the influence of CNCs in the solution absorption spectra for the CNC-RGO hybrids.
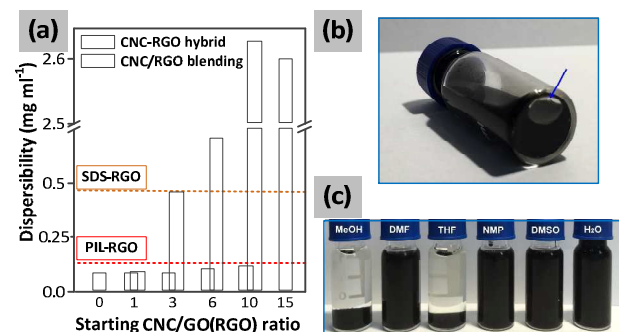
Figure 4. (a) Dispersibility of CNC/RGO blended samples and CNC-RGO hybrids. (b) No sediment was observed at the bottom of the vial, indicating the "true solution" character for the dispersions. (c) Digital photos of CNC-RGO 10 dispersed in various organic solvents through bath ultra-sonication.

The CNC-RGO hybrid (100 mg) with different coverage ratios was dispersed in water (10 mL) after sonication for 1 h; unstable CNC/RGO was removed by centrifugation at 5000 rpm for 20 min. The resulting supernatant was diluted, and measured by UV/vis spectroscopy to determine the maximum RGO concentration (**Fig. S2**). For comparisons, estimates were made of the maximum RGO concentration of the CNC/RGO blend samples with different starting CNC/RGO ratios, and with SDS-RGO and PIL-RGO contents. The data given in **Fig. 4 (a)** show that the maximum dispersibility of CNC/RGO blends increases slightly with increasing starting CNC/RGO ratio, indicating that RGO exfoliation by sonication in the presence of CNC is limited. As expected, the coverage ratio obviously affected the dispersibility of the CNC-RGO hybrids in aqueous solution, such that increasing the CNC significantly improved the dispersion ability of RGO, thus increasing the dispersibility of CNC-RGO. However, a remarkably high RGO concentration (>2.5 mg mL^{-1}) was obtained at a starting CNC/GO ratio ≥10, which was more than 5-fold and one order of magnitude larger than control samples for the SDS (0.46 mg mL^{-1}) and PIL (0.11 mg mL^{-1}) stabilizers. It is noted that the dispersion of CNC-RGO 10 appears stable indefinitely even at high concentrations ([CNC-RGO 10/water] = 10 mg mL^{-1}); samples prepared more than three months previously remain homogeneous without any CNC-RGO sedimentation (**Fig. 4 (b)**). The dispersibility of the CNC-RGO hybrid (CNC-RGO 10) was also tested in a series of solvents (10 mg mL^{-1}), including methanol, dimethyl formamide (DMF), tetrahydrofuran (THF), N-methyl-2-pyrrolidone (NMP) and dimethyl sulfoxide (DMSO). As shown in **Fig. 4 (c)**, CNC-RGO 10 is well-dispersed in solvents, such as DMF, NMP and DMSO, resulting in clear and homogeneous solutions. This result indicates that the dispersibility of the resulting CNC-RGO hybrids is strongly dependent on the nature of the covered CNC, which is similar to other covalently polymer-functionalized RGO.[46, 47]
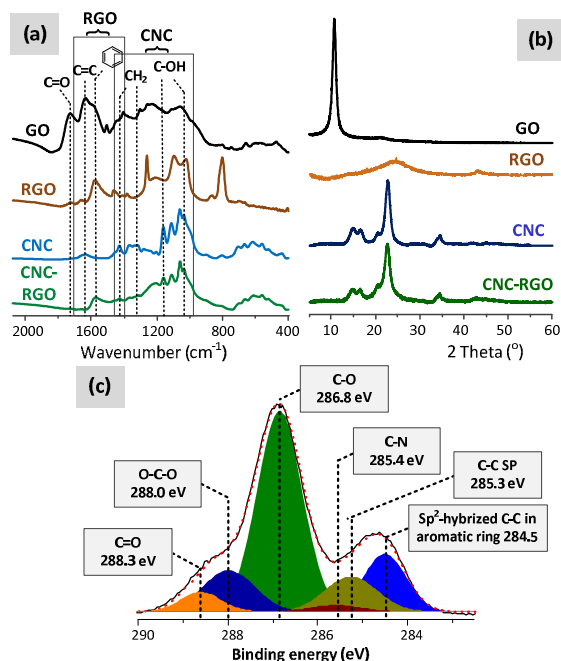

Figure 5. (a) FTIR spectra of GO, RGO, CNC and CNC-RGO hybrid. (b) XRD patterns of GO, RGO, CNC and CNC-RGO hybrid. (c) Carbon 1s XPS profile of CNC-RGO 10 hybrid.

That CNC was decorated on RGO surface was confirmed by FTIR, XPS and XRD spectra (**Fig. 5**). The FTIR spectra of GO shows C=O stretching vibration of –COOH and C-O vibration of epoxy/ether and alkoxide at 1734, 1264 and 1063 cm^{-1}.[16] A dramatic decrease in the peak intensities corresponding to the oxygen-containing functional groups is observed after the reduction of GO with hydrazine. For the CNC-RGO 10 hybrid, the FTIR spectrum shows peaks at 1161 and 1035 cm^{-1} associated with the hydroxyl groups of CNC. The XRD patterns of GO, RGO, CNC and CNC-RGO 10 were recorded, **Fig. 5 (b)**. The strong (002) diffraction peak of GO at 2Θ = 11.8° disappears in the RGO and CNC-RGO 10 samples after reduction. Four well-defined diffraction peaks at 14.9, 16.6, 22.7 and 34.5° correspond to the crystalline cellulose *I*β (defined by a triclinic cellulose *I*α and a monoclinic cellulose *I*β unit cell) appear in CNC and CNC-RGO 10, indicating that the crystalline structure of CNC-RGO 10 is undamaged after reduction with hydrazine.[48, 49] XPS were determined for the main elements and for the carbon-based bonds to further evaluate the chemical composition of the CNC-RGO hybrid. **Fig 5 (c)** shows the surface state of the CNC-RGO 10 hybrid, while GO and RGO are used for comparison in **Fig. S3**. The C 1s XPS spectrum of GO show peaks at 284.5, 286.3, 286.7 and 288.5 eV corresponding, respectively, to the non-oxygenated ring, C-O, epoxy/alkoxy and the carbonyl C=O bonds.[16] The significantly increased intensity of the four component peaks at 285.3, 286.8, 288.0 and 288.3 corresponding to C-C, C-O, O-C-O and O-C=O is evidence of the CNC structure covering on the RGO surface.[50]

The high dispersibility of the CNC-RGO hybrids in water or organic solvents, together their high thermal stability opens up

a range of potential applications. In this work, we examined the effect of electrical and mechanical reinforcement by incorporating the CNC-RGO hybrid into PEO by a simple blending process. CNC-RGO 10 having the optimum dispersibility and component ratio was chosen as the filler for preparation of PEO/CNC-RGO composites. Different weight ratios of CNC-RGO (1, 3, 5, 10, 15 wt.%) with concentrations of 10 mg mL^{-1} in water were added to aqueous PEO (10 wt.%) and stirred at 60 °C to form a stable dispersion. This mixture was then dropped into a Teflon mold and dried to obtain PEO and PEO/CNC-RGO films. For comparative purpose, we also introduced pristine CNC, SDS-RGO and PIL-RGO into the PEO matrix under the same conditions. All resulting PEO composite films were freestanding except for the PEO/SDS-RGO composite, which was unable to form a membrane.
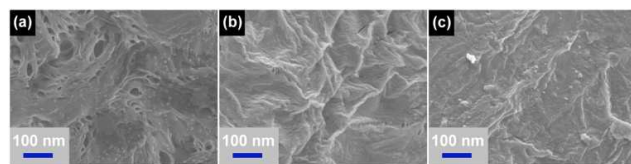

Figure 6. SEM images of (a) PEO/CNC 5 wt.%, (b) PEO/PIL-RGO 5 wt.% and (c) PEO/CNC-RGO 5 wt.%.
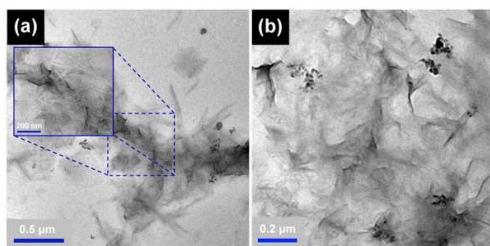

Figure 7. TEM images of PEO/CNC-RGO with (a) 3 and (b) 15 wt.% CNC-RGO hybrid.

The fracture surfaces of PEO composite membranes with 5 wt.% filler content after UV etching are shown in **Fig. 6**. The image of the PEO/CNC 5 wt.% composite shows homogeneous dispersion of CNC in PEO matrix, resulting from the formation of hydrogen bonds between the CNC and PEO matrix.[51, 52] The PEO/PIL-RGO 5 wt.% composite is randomly dispersed, as a 3D network, throughout the PEO matrix due to the presence of strong ionic interactions between PIL and PEO.[53, 54] For the PEO/CNC-RGO 5 wt.% composite, SEM images clearly show homogeneous dispersion of CNC with RGO sheets. TEM images of PEO/CNC-RGO composites with 3 and 15 wt.% CNC-RGO are shown in **Fig. 7**, which confirm the presence of randomly dispersed RGO sheets even at higher loadings (15 wt.%). Also, we found that RGO sheets were well covered by CNC whiskers (see dotted blue colour frame), which enhanced the compatibility of RGO with PEO matrix by hydrogen bonding between CNC and PEO.
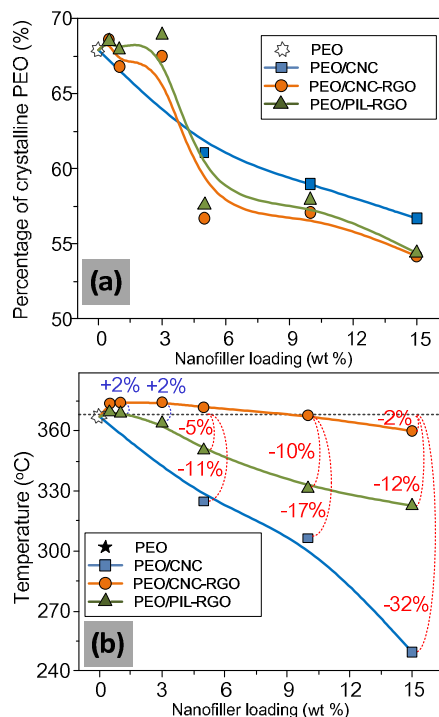

Figure 8. (a) Percent crystallinity *versus* nanofiller loading; and (b) T$_{d5}$ *versus* nanofiller loading.

The degrees of crystallinity and thermal stability of the PEO, PEO/PIL-RGO and PEO/CNC-RGO composites were determined using DSC and TGA, respectively. **Fig. 8 (a)** shows the crystallinity of PEO, PEO/PIL-RGO and PEO/CNC-RGO composites with various filler loadings. We can calculate the percentage of crystalline PEO (X_C) from: X_C (%)= $[\Delta H_m/(1-x)\Delta H^0_m] \times 100$, where ΔH^0_m is the melting enthalpy of a completely crystalline PEO sample (213.7 J g^{-1} for 100 % crystallinity), x is wt.% of filler in matrix, ΔH_m is the fusion heat of PEO/PIL-RGO or PEO/CNC-RGO composite (calculated from the integral area of the DSC curves).[55] By adding CNC whiskers, PIL-RGO or CNC-RGO sheets, the crystallinity of PEO is significantly reduced with increasing filler content and reaches a minimum (X_C = 54.2%) at a CNC-RGO content of 15 wt.%. This result shows that randomly dispersed CNC facilitates suppression of PEO crystallization - this effect was found to be heightened with PEO containing PIL-RGO or CNC-RGO. **Fig. 8 (b)** shows the temperature for the weight loss of the samples at 5% (T$_{d5}$) as a function of filler loading. In the PEO/CNC and PEO/PIL-RGO composites, T$_{d5}$ is significantly decreased with increasing filler content: the corresponding % enhancements are -32% and -12% for these composites with 15 wt.% filler loading, respectively. The TGA profiles (**Fig. S4**) show that PEO/CNC 15 wt.% and PEO/PIL-RGO 15 wt.% are less thermally stable, and have an obvious decomposition step from 200 to 350 °C due to the thermal degradation of less thermally stable filler structures. However, it is noteworthy that T$_{d5}$ is almost the same as that of pure PEO and is only slightly decreased even with high CNC-RGO loadings (15 wt.%). These results

indicate that the thermal stability of these PEO composites depends strongly on their incorporated nanofillers.
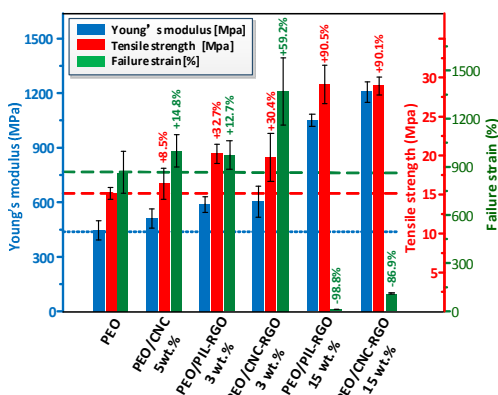

Figure 9. Mechanical properties of PEO, PEO/CNC, PEO/PIL-RGO and PEO/CNC-RGO composites.
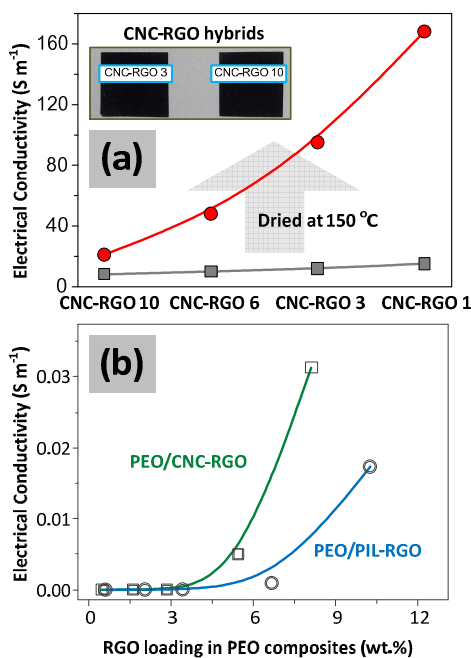

Figure 10. Electrical conductivity of (a) CNC-RGO hybrid, and (b) PEO/PIL-RGO and PEO/CNC-RGO composites with different RGO loadings (not including stabilizer).

The mechanical properties of PEO, PEO/CNC, PEO/PIL-RGO and PEO/CNC-RGO composites are shown in **Fig. S5** and **Fig 9**. Pristine PEO displayed typical yielding behavior with increasing stress during tension and corresponding Young's modulus (E_Y), tensile strength (σ_s) and failure strain (ε) are 447 MPa, 15.3 MPa and 863 %, respectively. Both E_Y and σ_s of PEO/CNC-RGO composites increase with CNC loading (**Fig. S5**). Compared to PEO containing CNC, the increase of E_Y and σ_s noted when adding graphene-based nanofillers into PEO are more significant than with other nanofillers, since graphene has very large elastic modulus (~1.0 TPa) and intrinsic strength (~130 GPa) values.[56] However, among these PEO/RGO composite

films, the increase in E_Y for the PEO/CNC-RGO composite is the most remarkable, where an improvement of 170 % (relative to pristine PEO) is achieved with 15 wt.% of CNC-RGO. This is largely attributed to the fact that E_Y of CNC stabilizer is much higher than that of PIL. The increase in ε, noted when adding nanofillers into the PEO, is significant at a relative low content of nanofiller in the PEO matrix. The maximum improvement in ε (59.2% in **Fig. 9**) is observed for the PEO/CNC-RGO 3 wt.% composite, which is ~5-fold greater than those for PEO/CNC 5 wt.% and PEO/PIL-RGO 3 wt.% composites. However, ε of PEO composites decrease with increasing nanofiller content from 5 to 15 wt.%, especially for the PEO/PIL-RGO composites, which drop to ~7% as the PIL-RGO content is increased to 10 wt.% (**Fig. S5**). **Fig. 9** and **Fig. S5** show that the optimized mechanical properties of these PEO composites can be achieved with a CNC-RGO content of 3 wt.%.

Since PEO is semi-crystalline, its mechanical properties depend strongly on the percentage of crystalline PEO (X_C), which is similar to semi-crystalline polyvinyl alcohol (PVA).[57] The DSC results show that X_C between PEO/PIL-RGO and PEO/CNC-RGO is less than 2% with same nanofiller loading, implying that the higher E_Y , σ_s and ε values found for the PEO composite are related to changes in the stabilizer. Hence, we can conclude that CNC covered RGO shows a synergism that yields a new kind of "hybrid nanofillers", which does not only significantly increase the E_Y and σ_s of PEO composites but also retain most of their ductility.

Fig. 10 (a) shows the electrical conductivities (σ) of CNC-RGO with various starting CNC/GO weight ratios. The electrical conductivity of CNC-RGO increases marginally with decreasing coverage ratios of CNC on the RGO surface with values close to other cellulose stabilized RGO composites (σ = ~24 S m⁻¹)[58]. It is noted that CNC-RGO can form free-standing films (see inset photos in **Fig. 10 (a)**), which may result from the CNC having easy film-formation properties, but PIL-RGO cannot. When the CNC-RGO films were dried at 150 °C for 12 h under Ar gas, their electrical conductivity was improved, especially for CNC-RGO hybrids with low CNC coverage ratios. The electrical conductivity of CNC-RGO 1 (σ = 162 S m⁻¹) dried in this way was ~10 times higher than for films which were air-dried at 70 °C due to the formation of tight RGO stacking after Ar-drying at 150 °C.[29] However, there is no obvious change in CNC-RGO 10 hybrid dried in this way, which may be attributable to CNC-RGO 10 being covered with a dense CNC network, in which the dense CNC prevents the RGO sheets packing tighter than the air-dried counterpart. For PEO composites, the conductivity of PEO/PIL-RGO and PEO/CNC-RGO films increases with increasing RGO contents, (see **Fig. 10 (b)**), leading to a sharp increase in electrical conductivity as RGO exceeds 5 wt.%, *i.e.,* an increase of about 1~2 orders of magnitude. This result indicates that PEO composites with high RGO contents induce the formation of electrically conductive networks that provide good interconnectivity for electron transfer.[19, 59]

In this study, CNC was used as a stabilizer to decorate RGO sheets in an approach designed to reduce toxicity as its goal in the preparation of stable aqueous RGO dispersions. However,

the common reductant used in chemical reduction of GO is hydrazine, which is highly toxic. Hence, we used hydrothermal dehydration, an environmentally friendly approach to replace chemical reduction of GO in hydrazine.[60] We also studied the efficacy of CNC by examining different CNC/GO weight ratios. **Fig. S6** shows the dispersibility of the resulting CNC-RGO hybrids (denoted as CNC-RGO$_{HT}$) after hydrothermal reaction. As expected, the starting GO/CNC weight ratio strongly affects the dispersibility of aqueous CNC-RGO$_{HT}$ and the stability of RGO dispersion can be obtained with starting CNC/GO weight ratios >3. TGA, UV/vis and Raman spectroscopy were used to characterize the resulting CNC-RGO$_{HT}$ with a starting CNC/RGO ratio of 10 (denoted as CNC-RGO$_{HT}$ 10) (**Table 1** and **Fig. S6**). The results show that the coverage ratio and aqueous RGO dispersion of CNC-RGO$_{HT}$ were 43.5 % and >2.5 mg mL^{-1} respectively, which are similar to those of hydrazine-reduced CNC-RGO 10 (**Table 1**). Raman spectra show that the intensity ratio (I_D/I_G) of the D band to G band of the CNC-RGO$_{HT}$ 10 was about 1.02, which is lower than those of hydrazine-reduced RGO and CNC-RGO 10 (I_D/I_G = 1.21). This result indicates that fewer defects are produced after removal of oxygen moieties by hydrothermal reduction, which agrees well with a previous report.[60]
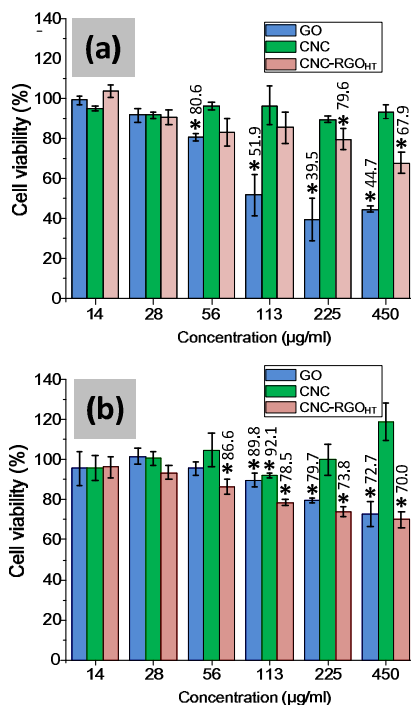

Figure 11. Cell viability of (a) A375 and (b) HepG 2 cells exposed to GO, CNC and CNC-RGO$_{HT}$ obtained by CCK-8. Results are expressed as means ± SD (error bars), n=3, *p < 0.05 compared to mean values of the blank control group (student's t-test).

The biocompatibility of CNC-RGO$_{HT}$ was evaluated by measuring cell viability using a Cell Counting Kit-8 (CCK-8). The viabilities of human melanoma A375 cells and human liver cancer (HepG-2 cells) were assessed after a 24 h exposure to

GO, CNC and CNC-RGO$_{HT}$ 10 (**Fig. 11**). Cell viabilities of A375 and HepG-2 cells, after incubation with 450 μl mL^{-1} CNC, were 93% and 119 %, respectively, compared with the blank group. When exposed to GO at concentration of 450 μl mL^{-1}, the cell viabilities decreased to 45 % and 73 %, respectively, in a dose-dependent manner. However, the cell viability of A375 cells after exposure to 450 μl mL^{-1} CNC-RGO$_{HT}$ was 68 %, which was higher than those exposed to GO. The toxicity of CNC-RGO$_{HT}$ was also compared with that cited in a previous report for mammalian A549 cells exposed to RGO (cell viability of <20% at 85 μl mL^{-1}) while HeLa cells exposed to RGO containing surfactants [Trition X-100, SDS and cetyltrimethylammonium bromide (CTAB)] (cell viability of <20% at 450 μl mL^{-1}) were quantified by CCK-8 assay.[20] The relative toxicity of these RGOs was much higher than that of CNC-RGO$_{HT}$ probably due to the high toxicity of the reductant and surfactants to the mammalian cell lines. Hence, CNC was used as a stabilizer to prepare CNC-RGO hybrids which, when combined with the hydrothermal reduction method, enabled fabrication of biocompatible RGO with a high water solubility.

Conclusions

In conclusion, by utilizing CNC as a stabilizer, we have created an effective and scalable process to prepare stable high concentration aqueous RGO dispersions. The combination of high dispersibility, good processability, tunable electric conductivity and high thermal stability makes the CNC decorated RGO promising in a wide range of applications. The sandwich-like structure formed with the hydrophilic surface of CNC facilitates dispersion in the PEO matrix using a simple procedure. The PEO composite films containing CNC decorated RGO show synergistic effects with superior mechanical and thermal properties when compared to PEO composite films which are enhanced by polymeric stabilized RGO and pristine CNC. Optimal mechanical properties of PEO/CNC-RGO were achieved with CNC-RGO content of 3 wt.%, which not only significantly enhanced E_Y and $σ_s$ of PEO composites, but also allowed them retain most of their ductility. The CNC stabilizer used in this work can be extended to obtain stable dispersions of RGO sheets in a green approach (hydrothermal dehydration route), which will promote the usage of CNC-RGO hybrids for electronic devices and as biocompatible materials.

Experimental

Materials

Graphite particles (average size 30 μm, Fluka) were used as received. Graphene oxide (GO) and PIL(Br), poly(1-vinyl-3-butylimidazolium) bromide were synthesized according to our previously published reports.[19, 61] Microcrystalline cellulose, sodium dodecyl sulphate (SDS), sulphuric acid and (3-(4,5-dimethylthiazol-2-yl)-2,5-diphenyl tetrazolium bromide) (CCK-8) were purchased from Sigma-Aldrich. N,N'-dimethyl formamide (DMF) (94%), tetrahydrofuran (THF) (99.6%, Acros), N-methyl-2-pyrrolidinone (NMP) (99.5%, Acros), methanol

(MeOH) (99.9%, Acros) and dimethyl sulfoxide (DMSO) (99.9%) were dried and distilled prior to use.

Synthesis of cellulose nanocrystals (CNC)

CNC were extracted from microcrystalline cellulose by acidic hydrolysis with sulfuric acid according to a protocol reported elsewhere.[44] Hydrolysis was conducted with 64% (w/w) sulfuric acid at 45 °C for 45 min with vigorous stirring. After removing the acid, dialysis (membrane Spectra/Por 2, MWCO 12,000-14,000) and ultrasonic treatment were performed. Finally, the CNC were freeze-dried and stored until use.

Synthesis of CNC-RGO

Hydrazine-reduced CNC-RGO: Dried CNC (0.5 g) were dispersed in 100 mL water and subsequently ultrasonicated for 15 min. After addition of GO (at 5 mg mL^{-1}), the CNC/GO suspension was heated to 100 °C under stirring. Then hydrazine (50 %) (0.5 mL for 100 mg GO) was added to the mixture slowly under nitrogen atmosphere. The reaction was allowed to proceed under stirring 100 °C for 1 h. After cooling, the resulting CNC-RGO were purified via re-dispersion under sonication and centrifugation at 13,000 rpm for 30 min 3~5 times. The final product was obtained by freeze-drying.

Hydrothermal reduced CNC-RGO (CNC-RGO$_{HT}$): A total of 100 mL of 2 mg mL^{-1} CNC/GO aqueous solution with various starting CNC/GO weight ratios was transferred to a Teflon-lined autoclave and heated at 180 °C for 6 h. The purification was similar to the preparation of hydrazine-reduced CNC-RGO hybrids.

Synthesis of SDS-RGO and PIL-RGO

To prepare the PIL-RGO, 1 g of PIL were dissolved in water and added to 50 mL (2 mg mL^{-1}) of an aqueous GO suspension. The mixture was then reduced with hydrazine (0.5 mL) at 100 °C for 1 h under continuous stirring. After reduction, a dispersion of PIL-RGO was centrifuged at 13,000 rpm for 30 min 3~5 times to residual PIL and then freeze-dried to obtain the final product. SDS-RGO was synthesized *via* the same procedure, but replacing PIL by SDS and without purification.

Preparation of PEO/PIL-RGO and PEO/CNC-RGO composites

PEO with a M_w of 600,000 g mol^{-1} was dissolved in RO water with a concentration of 10 wt.% at 80 °C for 2 h. The PIL-RGO or CNC-RGO suspension (5 mg mL^{-1}) was gradually dropped into the mechanical stirred PEO solution with specified amounts. The predetermined weight contents of the PIL-RGO or CNC-RGO in the PEO composite films were 0.5, 1, 3, 5, 10 and 15 wt.%. The mixtures were stirred (600 rpm) at 60 °C for 6 h. Then PEO/PIL-RGO or PEO/CNC-RGO were cast and dried in an oven at 60 °C for 24 h.

Characterization

The thermal degradation behavior was recorded on a Q50 thermogravimetric analyzer (TGA) in a nitrogen atmosphere at 10 °C min^{-1} from room temperature to 850 °C. Raman spectra were measured using a Nicolet IS-10 Raman microprobe with a 532 nm argon ion laser. The degree of crystallinity was investigated by differential scanning calorimetry (DSC Q2000) at a heating rate of

10 °C min^{-1} from -90 °C to 150 °C. X-ray diffraction (XRD) studies were conducted on a Bruker D8 Advance diffractometer with Cu-Kα radiation at a scan rate of 2° min^{-1} from 2° to 90°. Transmission eletron microscopy (TEM) using a JEOL JEM-1200CX-11 at 120 kV was employed to ascertain the morphology of CNC-RGO hybrids. Scanning electron microscopy (SEM) was imaged with a Hitachi S-4700 microscope at 15 kV. FTIR spectra were recorded with a Nicolet Avatar 320 FTIR spectrometer by depositing solution on salt plates. X-ray photoelectron spectroscopy (XPS) analysis was performed on an ESCA 2000 (VG Microtech) with a mono-chromatized Al Kα anode. UV-vis detection was conducted on a HP8452A (Hewlett-Packard) diode-array spectrophotometer. The electrical conductivity of the CNC-RGO hybrids and PEO/CNC-RGO composite films was measured by a standard four-probe method.

Cell culture

Human melanoma cells (A375 cell line, Shanghai Maisha Biotechnology Co. Ltd., Shanghai, China) and human liver cancer cells (HepG-2 cell line, Shanghai Maisha Biotechnology Co. Ltd., Shanghai, China) were cultured in Dulbecco's modified Eagle's medium (DMEM) supplemented with 10 % fatal bovine serum (FBS, Gibco, USA) and 1 % penicillin-streptomycin (Hyclone, USA). Cells were maintained at 37 °C in a humidified incubator (Heraeus, Germany) with 5% CO$_2$.

CCK-8 assay for cytotoxicity test

The cytotoxicity of blank (normal saline, NS), GO, CNC and CNC-RGO$_{HT}$ 10 was measured by CCK-8 (Dojindo Molecular Technology, Gaithersburg, MD) assay following the manufacturer's instructions. Cells were seeded to 96-well plates to settle overnight. They were washed with PBS (phosphate buffer saline) and fresh fatal bovine serum-free culture medium was added, then incubated with different concentrations (14, 28, 56, 113, 225 and 450 µl mL^{-1}) of all the samples for the next 24 h. After incubation, the cells were washed with PBS, fresh culture medium without fatal bovine serum and 10 µL CCK-8 solution were added to each well. After 1.6 h incubation at 37 °C, the absorbance of each well was measured at 450 nm by using a micro-plate reader (Tecan Austria GmbH, 5082 Grodig, Austria).

Notes and references

1. V. Georgakilas, M. Otyepka, A. B. Bourlinos, V. Chandra, N. Kim, K. C. Kemp, P. Hobza, R. Zboril and K. S. Kim, *Chem Rev*, 2012, 112, 6156-6214.
2. Z. Wang, X. Z. Tang, Z. Z. Yu, P. Guo, H. H. Song and X. S. Duc, *Chin J Polym Sci*, 2011, 29, 368-376.
3. Y. Zhu, S. Murali, W. Cai, X. Li, J. W. Suk, J. R. Potts and R. S. Ruoff, *Adv Mater*, 2010, 22, 3906-3924.

4.   C. K. Chua and M. Pumera, *Chem Soc Rev*, 2014, 43, 291-312.
5.   R. K. Layek and A. K. Nandi, *Polymer*, 2013, 54, 5087-5103.
6.   Y. Liang, D. Wu, X. Feng and K. Müllen, *Adv Mater*, 2009, 21, 1679-1683.
7.   Y. Xu, H. Bai, G. Lu, C. Li and G. Shi, *J Am Chem Soc*, 2008, 130, 5856-5857.
8.   R. Hao, W. Qian, L. Zhang and Y. Hou, *Chem Commun*, 2008, 48, 6576-6578.
9.   S. Stankovich, R. D. Piner, X. Chen, N. Wu, S. T. Nguyen and R. S. Ruoff, *J Mater Chem*, 2006, 16, 155-158.
10.   H. Bai, Y. Xu, L. Zhao, C. Li and G. Shi, *Chem Commun*, 2009, 13, 1667-1669.
11.   E. Y. Choi, T. H. Han, J. Hong, J. E. Kim, S. H. Lee, H. W. Kim and S. O. Kim, *J Mater Chem*, 2010, 20, 1907-1912.
12.   X. Qi, K. Y. Pu, H. Li, X. Zhou, S. Wu, Q. L. Fan, B. Liu, F. Boey, W. Huang and H. Zhang, *Angew Chem Int Edit*, 2010, 49, 9426-9429.
13.   A. J. Patil, J. L. Vickery, T. B. Scott and S. Mann, *Adv Mater*, 2009, 21, 3159-3164.
14.   S. Wang, H. Li, L. Zhang, B. Li, X. Cao, G. Zhang, S. Zhang and L. Wu, *Chem Commun*, 2014, 50, 9700-9703.
15.   T. Kim, H. Lee, J. Kim and K. S. Suh, *ACS Nano*, 2010, 4, 1612-1618.
16.   Y. S. Ye, C. Y. Tseng, W. C. Shen, J. S. Wang, K. J. Chen, M. Y. Cheng, J. Rick, Y. J. Huang, F. C. Chang and B. J. Hwang, *J Mater Chem*, 2011, 21, 10448-10453.
17.   C. C. Teng, C. C. M. Ma, C. H. Lu, S. Y. Yang, S. H. Lee, M. C. Hsiao, M. Y. Yen, K. C. Chiou and T. M. Lee, *Carbon*, 2011, 49, 5107-5116.
18.   Z. Liu, J. Liu, L. Cui, R. Wang, X. Luo, C. J. Barrow and W. Yang, *Carbon*, 2013, 51, 148-155.
19.   H. Wang, S. G. Bi, Y. S. Ye, Y. Xue, X. L. Xie and Y. W. Mai, *Nanoscale*, 2015, 7, 3548-3557.
20.   Y. K. Kim, M. H. Kim and D. H. Min, *Chem Commun*, 2011, 47, 3195-3197.
21.   C. Cheng, S. Li, S. Nie, W. Zhao, H. Yang, S. Sun and C. Zhao, *Biomacromolecules*, 2012, 13, 4236-4246.
22.   C. Cheng, S. Li, J. Zhao, X. Li, Z. Liu, L. Ma, X. Zhang, S. Sun and C. Zhao, *Chem Eng J*, 2013, 228, 468-481.
23.   J. Zhang, H. Yang, G. Shen, P. Cheng, J. Zhang and S. Guo, *Chem Commun*, 2010, 46, 1112-1114.
24.   J. Gao, F. Liu, Y. Liu, N. Ma, Z. Wang and X. Zhang, *Chem Mater*, 2010, 22, 2213-2218.
25.   Y. Lei, Z. Tang, R. Liao and B. Guo, *Green Chemistry*, 2011, 13, 1655-1658.
26.   J. Li, G. Xiao, C. Chen, R. Li and D. Yan, *J Mater Chem A*, 2013, 1, 1481-1487.
27.   Y. Wang, P. Zhang, C. Fang Liu, L. Zhan, Y. Fang Li and C. Z. Huang, *RSC Adv*, 2012, 2, 2322-2328.
28.   C. Zhu, S. Guo, Y. Fang and S. Dong, *ACS Nano*, 2010, 4, 2429-2437.
29.   S. Park, J. An, I. Jung, R. D. Piner, S. J. An, X. Li, A. Velamakanni and R. S. Ruoff, *Nano Lett*, 2009, 9, 1593-1597.
30.   S. Stankovich, R. D. Piner, S. T. Nguyen and R. S. Ruoff, *Carbon*, 2006, 44, 3342-3347.
31.   R. J. Moon, A. Martini, J. Nairn, J. Simonsen and J. Youngblood, *Chem Soc Rev*, 2011, 40, 3941-3994.
32.   M. A. S. Azizi Samir, F. Alloin and A. Dufresne, *Biomacromolecules*, 2005, 6, 612-626.
33.   C. Z. Geng, X. Hu, G. H. Yang, Q. Zhang, F. Chen and Q. Fu, *Chin J Polym Sci*, 2015, 33, 61-69.
34.   Y. Habibi, L. A. Lucia and O. J. Rojas, *Chem Rev*, 2010, 110, 3479-3500.
35.   P. M. Carrasco, S. Montes, I. García, M. Borghei, H. Jiang, I. Odriozola, G. Cabañero and V. Ruiz, *Carbon*, 2014, 70, 157-163.
36.   C. Olivier, C. Moreau, P. Bertoncini, H. Bizot, O. Chauvet and B. Cathala, *Langmuir*, 2012, 28, 12463-12471.
37.   H. Zhu, Y. Li, Z. Fang, J. Xu, F. Cao, J. Wan, C. Preston, B. Yang and L. Hu, *ACS Nano*, 2014, 8, 3606-3613.
38.   Y. Li, H. Zhu, F. Shen, J. Wan, S. Lacey, Z. Fang, H. Dai and L. Hu, *Nano Energy*, 2015, 13, 346-354.
39.   A. Carlmark, E. Larsson and E. Malmström, *Eur Polym J*, 2012, 48, 1646-1659.
40.   D. Roy, M. Semsarilar, J. T. Guthrie and S. Perrier, *Chem Soc Rev*, 2009, 38, 2046-2064.
41.   A. Isogai, T. Saito and H. Fukuzumi, *Nanoscale*, 2011, 3, 71-85.
42.   J. Majoinen, A. Walther, J. R. McKee, E. Kontturi, V. Aseyev, J. M. Malho, J. Ruokolainen and O. Ikkala, *Biomacromolecules*, 2011, 12, 2997-3006.
43.   A. Kundu, R. K. Layek and A. K. Nandi, *Journal of Materials Chemistry*, 2012, 22, 8139-8144.
44.   M. Roman and W. T. Winter, *Biomacromolecules*, 2004, 5, 1671-1677.
45.   Y. S. Ye, H. Wang, S. G. Bi, Y. Xue, Z. G. Xue, Y. G. Liao, X. P. Zhou, X. L. Xie and Y. W. Mai, *Carbon*, 2015, 86, 86-97.
46.   Y. S. Ye, Y. N. Chen, J. S. Wang, J. Rick, Y. J. Huang, F. C. Chang and B. J. Hwang, *Chem Mater*, 2012, 24, 2987-2997.
47.   L. Kan, Z. Xu and C. Gao, *Macromolecules*, 2010, 44, 444-452.
48.   K. K. Sadasivuni, A. Kafy, L. Zhai, H. U. Ko, S. Mun and J. Kim, *Small*, 2015, 11, 994-1002.
49.   K. Fleming, D. G. Gray and S. Matthews, *Chemistry – A European Journal*, 2001, 7, 1831-1836.
50.   X. Cao, Y. Habibi and L. A. Lucia, *J Mater Chem*, 2009, 19, 7137-7145.
51.   D. Cheng, Y. Wen, L. Wang, X. An, X. Zhu and Y. Ni, *Carbohydr Polym*, 2015, 123, 157-163.
52.   M. Pereda, N. E. Kissi and A. Dufresne, *ACS Appl Mater Interfaces*, 2014, 6, 9365-9375.
53.   Y. S. Ye, J. Rick and B. J. Hwang, *J Mater Chem A*, 2013, 1, 2719-2743.
54.   Y. S. Ye, H. Wang, S. G. Bi, Y. Xue, Z. G. Xue, X. P. Zhou, X. L. Xie and Y. W. Mai, *J Mater Chem A*, 2015, 3, 18064-18076.
55.   H. Zhang, S. Kulkarni and S. L. Wunder, *J Phys Chem B*, 2007, 111, 3583-3590.
56.   C. Lee, X. Wei, J. W. Kysar and J. Hone, *Science (80)*, 2008, 321, 385-388.
57.   Y. S. Ye, M. Y. Cheng, X. L. Xie, J. Rick, Y. J. Huang, F. C. Chang and B. J. Hwang, *J Power Sources*, 2013, 239, 424-432.
58.   A. G. Nandgaonkar, Q. Wang, K. Fu, W. E. Krause, Q. Wei, R. Gorga and L. A. Lucia, *Green Chemistry*, 2014, 16, 3195-3201.
59.   J. H. Yang, S. H. Lin, Y. D. Lee, *J Mater Chem*, 2012, 22, 10805-10815.
60.   Y. Zhou, Q. Bao, L. A. L. Tang, Y. Zhong and K. P. Loh, *Chem Mater*, 2009, 21, 2950-2956.

61.   Y. S. Ye, X. L. Xie, J. Rick, F. C. Chang and B. J. Hwang, *J Power Sources*, 2014, 247, 991-998.

Green Chemistry Accepted Manuscript
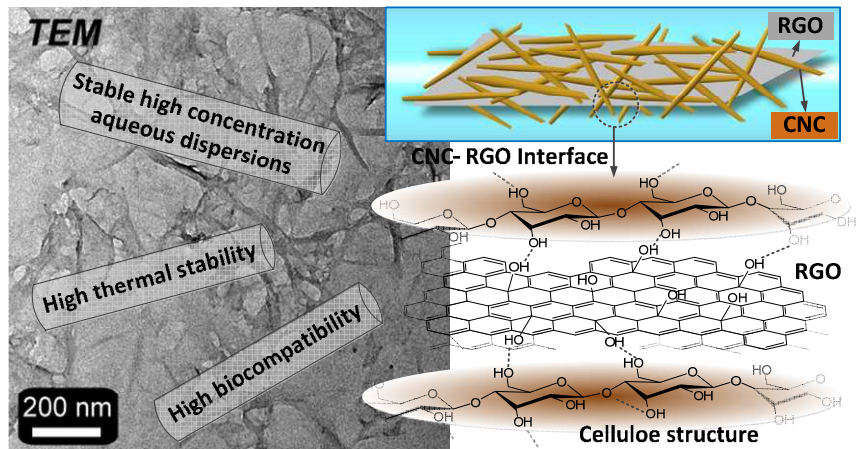
Graphical Abstract

The hydrothermal dehydration of GO to RGO, using biodegradable and renewable materials such as CNC, offers a sustainable approach to large-scale preparation of highly biocompatible and easily dispersed RGO for a range of applications.